

Adjoint Methods for Guiding Adaptive Mesh Refinement in Tsunami Modeling

B. N. Davis and R. J. LeVeque

the date of receipt and acceptance should be inserted later

Abstract One difficulty in developing numerical methods for tsunami modeling is the fact that solutions contain time-varying regions where much higher resolution is required than elsewhere in the domain, particularly when tracking a tsunami propagating across the ocean. The open source GeoClaw software deals with this issue by using block-structured adaptive mesh refinement to selectively refine around propagating waves. For problems where only a target area of the total solution is of interest (e.g. one coastal community), a method that allows identifying and refining the grid only in regions that influence this target area would significantly reduce the computational cost of finding a solution.

In this work, we show that solving the time-dependent adjoint equation and using a suitable inner product with the forward solution allows more precise refinement of the relevant waves. We present the adjoint methodology first in one space dimension for illustration and in a broad context since it could also be used in other adaptive software, and potentially for other tsunami applications beyond adaptive refinement. We then show how this adjoint method has been integrated into the adaptive mesh refinement strategy of the open source GeoClaw software and present tsunami modeling results showing that the accuracy of the solution is maintained and the computational time required is significantly reduced through the integration of the adjoint method into adaptive mesh refinement.

1 Introduction

Adjoint methods are often used in conjunction with the numerical solution of differential equations for a variety of purposes, such as computing sensitivities of the solution to input data, solving inverse problems, estimating errors in the solution, or guiding the design of a computational grid to most efficiently compute particular quantities of interest. We are exploring the use of adjoint methods in tsunami modeling by incorporating them into the open source GeoClaw software

Supported in part by an NSF Graduate Research Fellowship DGE-1256082 and NSF grants DMS-1216732 and EAR-133141.

Department of Applied Mathematics, University of Washington, Seattle, WA.

that is widely used for tsunami simulation, see e.g. Berger et al (2011); GeoClaw Development Team (Accessed 2016); LeVeque et al (2011). We mention several other potential applications below, but in this paper we focus primarily on one particular use: guiding adaptive mesh refinement (AMR) to efficiently capture the waves from a far-field tsunami that will impact a particular “target location,” by which we mean a specific location where we want to compare with available DART buoy or tide gauge data, or a portion of the coastline where we wish to compute inundation, for example.

GeoClaw simulations often use 6 or 7 nested levels of refinement, starting with a resolution of 1 or 2 degrees of latitude/longitude over the entire computational domain. This might be refined to 4-minute or 1-minute resolution around the propagating waves, and then refined to successively higher resolution around the target region, where the finest grids may be 1/3 arcsecond for inundation studies. The target location where the highest levels of refinement is required can be specified directly by the user. In this paper we are concerned with the question of how best to refine the ocean to capture the portions of the propagating tsunami that will eventually impact this location, without over-refining waves that will not.

Refining the wave as it propagates across the ocean can be automated in GeoClaw, by refining only in regions where the surface elevation differs from sea level above some specified tolerance. Every few time steps recursive regridding is performed in which all such points on a given grid are flagged for refinement to the next level and the flagged points are clustered into rectangular patches using the algorithm of Berger and Rigoutsos (1991). Refinement “regions” can also be specified, space-time subsets of the computational domain where refinement above a certain level can be either required or forbidden. This is used to allow the finest levels of refinement only near the target location. These AMR regions can also be used to induce the code to follow only the waves of interest as the tsunami propagates across the ocean, but to do so optimally often requires multiple attempts and careful examination of how the solution is behaving, generally using coarser grid runs for guidance. This manual guiding of AMR may also fail to capture some waves that are important. For example, a portion of a tsunami wave may appear to be heading away from the target location but might later reflect off a distant shoreline or underwater feature, or edge waves may be excited that propagate back and forth along the continental shelf for hours after the primary wave has passed.

This challenge in tsunami modeling was the original motivation for our work on adjoint-based refinement, which we are also incorporating into the more general Clawpack software (Clawpack Development Team (2015)), which solves general hyperbolic partial differential equations that arise in many wave propagation problems. GeoClaw is based on the AMRClaw branch of Clawpack, a more general code that implements adaptive mesh refinement in both two and three space dimensions. Other applications where adjoint-based refinement could be very useful include earthquake simulation, for example, where the desire might be to efficiently refine only the seismic waves that will reach a particular location.

For a time-dependent partial differential equations such as the shallow water equations, we generally wish to solve a “forward problem” in which initial data is specified (e.g. sea floor displacement due to an earthquake) at some initial time t_0 and the problem is solved forward in time to find the effect at the target location at some later time t_f . The *adjoint equation* is a closely related partial differential equation that must be solved *backwards* in time from the final time t_f to the

initial time, as derived in Section 3. The data for the adjoint equation (specified at the final time) typically approximates a delta function at the target location. This spreads out into waves as the adjoint equation is solved backward in time, with the same bathymetry-dependent wave speed \sqrt{gh} as in the linearized forward problem. The key idea is that at any intermediate time t between t_0 and t_f , the only regions in space where the forward solution could possibly reach the target location at time t_f are regions where the adjoint solution is nonzero. Moreover by computing a suitable inner product of the forward and adjoint solutions at time t , it is possible to determine whether the forward solution wave at a given spatial point will actually reach the target location, or whether it can be safely ignored. This information can then be used to decide whether or not to refine this spatial location in the forward solution.

In Section 2 we briefly introduce the mathematical concept of an adjoint equation. Then in Section 3 we derive the adjoint equation for the linearized shallow water equations in one space dimension and illustrate the main idea used in adjoint-based refinement in this simple context before extending to the two-dimensional problem in Section 5. In Section 6 we illustrate the use of this method and its efficiency on a tsunami modeling problem using GeoClaw.

2 Adjoint equation for a system of equations

For readers not familiar with the concept of an adjoint equation, it may be easiest to appreciate the power and limitations of this approach by first considering the solution to an algebraic system of equations, beginning with a linear system of the form $Ax = b$, where A is an invertible $n \times n$ matrix, b is a given vector with n components, and the solution is $x = A^{-1}b$. In practice such a system is best solved by Gaussian elimination, requiring $\mathcal{O}(n^3)$ operations. Suppose that we are not interested in the full solution x but only in one component, say x_k . In general we must still solve the full system to determine x_k . But now suppose we want to do this for many different sets of data b , or that we wish to determine the sensitivity of x_k to changes in any component of b . In these situations the adjoint equation can be very useful since it requires solving only a single system of equations rather than many systems.

More generally, suppose that we only care about $J = \phi^T x = \sum_{i=1}^n \phi_i x_i$, where ϕ is some specified vector with n components. In particular if ϕ is the unit vector with $\phi_k = 1$ and $\phi_i = 0$ for $i \neq k$, then $\phi^T x = x_k$, the case considered in the previous paragraph. The adjoint approach works for more general ϕ , i.e. when we only care about some scalar quantity of interest that can be defined as a linear functional applied to x .

For the linear system $Ax = b$, the adjoint equation is the linear system $A^T \hat{x} = \phi$, where the vector ϕ is now used as the data on the right hand side and we solve for \hat{x} , the adjoint solution. The matrix A^T is the transpose (also called the adjoint) of the matrix A , with elements $(A^T)_{ij} = A_{ji}$. This is also an $n \times n$ invertible matrix so this problem has a unique solution $\hat{x} = A^{-T} \phi$. The matrix A^{-T} is the inverse of the transpose, which agrees with the transpose of the inverse.

The adjoint solution can now be used to compute $J(b)$, the value of the functional $\phi^T x$, where x solves $Ax = b$, by using elementary linear algebra:

$$J(b) = \phi^T x = \phi^T A^{-1} b = (A^{-T} \phi)^T b = \hat{x}^T b. \quad (1)$$

Note that once we have solved the adjoint equation for \hat{x} , we can compute $J(b)$ for *any* data b without solving additional linear systems. We need only compute the inner product $\hat{x}^T b = \sum_{i=1}^n \hat{x}_i b_i$, which requires only $\mathcal{O}(n)$ operations.

Moreover, we can also compute the sensitivity of $J(b)$ to a change in any component b_i of the data. Differentiating (1) with respect to b_i shows that

$$\frac{\partial J(b)}{\partial b_i} = \hat{x}_i, \quad (2)$$

in other words the components of the adjoint solution are exactly the sensitivities of J to changes in the corresponding component of b . We could have estimated the sensitivity $\partial J(b)/\partial b_i$ by varying b_i slightly and solving a perturbed linear system, but we would have had to solve n such linear systems to estimate all the sensitivities. The adjoint equation computes them all simultaneously through the solution of a single linear system.

In tsunami modeling we may wish to compute the sensitivity of the tsunami observed at our target location to changes in the data, e.g. to changes in the seafloor deformation if we are using a gradient-based optimization algorithm to solve an inverse problem to match observations (see Blaise et al (2013) for one such application to tsunami source inversion). Or we may want to determine what potential source regions around the Pacific Rim give the largest tsunami response at a particular target location (such as Pearl Harbor, as considered in a study by Tang et al (2006)). Rather than solving many forward problems, this can be determined with a single adjoint solution.

One limitation of the adjoint approach is that changing the target location is analogous to changing the vector ϕ defining the quantity of interest $J(b)$ in the linear system problem, and a new adjoint solution must be computed for each location of interest.

Another limitation is that the adjoint approach is most easily applied to a linear problem. If we replace the linear system $Ax = b$ by a nonlinear system of equations $f(x) = b$ that defines x for data b , then we can still use an adjoint approach to compute sensitivities of $J(b) = \phi^T x$ to changes in b , but we must first linearize about a particular set of data \bar{b} with solution \bar{x} and can only compute sensitivities due to small changes in b around \bar{b} . The adjoint equation then takes the form of a linear system where the matrix A is replaced by the Jacobian matrix of the function f evaluated at \bar{x} .

The GeoClaw software solves the nonlinear shallow water equations, but in this paper we restrict our attention to the above-mentioned application of tracking waves in the ocean that will reach the target location. Since a tsunami in the ocean typically has an amplitude that is very small compared to the ocean depth, these equations essentially reduce to the linear shallow water equations and the adjoint equation linearized about the ocean at rest is sufficient for our needs. We will see in Section 3 that these adjoint equations take a very similar form to the linearized shallow water equations, although with slightly different boundary conditions. If we wanted to compute sensitivities of the nonlinear onshore inundation to changes in data then we would have to linearize about a particular forward solution. In Section 8 we make some additional comments about extension to nonlinear problems.

Adjoint equations have been used computationally for many years in a variety of different fields, with wide ranging applications. A few examples include

weather model tuning (Hall (1986)), aerodynamics design optimization (e.g. Giles and Pierce (2000); Jameson (1988); Kennedy and Martins (2013)), automobile aerodynamics (Othmer (2014)), and geodynamics (Bunge et al (2003)). They have been used for seismic inversion (e.g. Akcelik et al (2002); Tromp et al (2005)) and recently also applied to tsunami inversion (Blaise et al (2013)). The adjoint method has also been used for error estimation in the field of aerodynamics (Becker and Rannacher (2001)) and for general coupled time-dependent systems (Asner et al (2012)). Various solution methods have been combined with adjoint approaches, including Monte Carlo (Buffoni and Cupini (2001)), finite volume (Mishra et al (2013)), finite element (Asner et al (2012)), and spectral-element (Tromp et al (2005)) methods.

It is also possible to use adjoint equations to compute sensitivities of J to changes in the input data. This has led to the adjoint equations being utilized for system control in a wide variety of applications such as shallow-water wave control by Sanders and Katopodes (2000) and optimal control of free boundary problems by Marburger (2012). This is also useful in solving inverse problems and potential applications of this approach in tsunami modeling are being studied separately.

The adjoint method has also been used to guide adaptive mesh refinement, typically by estimating the error in the calculation and using that to determine how to adjust the grid. Leveraging the adjoint problem to achieve this goal is not a new concept, and has been explored significantly for steady state problems where work has been done to guide AMR (e.g. Pierce and Giles (2000); Becker and Rannacher (2001); Venditti and Darmofal (2000, 2002); Park (2004); Venditti and Darmofal (2003)), and put error bounds on solution accuracy (e.g. Giles and Suli (2002)). In the finite volume literature this approach is known as *adjoint-error* based mesh adaptation, although perhaps a clearer term would be *adjoint-error* based mesh adaptation. Within the finite volume community output-based mesh refinement has begun to be used for unsteady problems. Specifically, temporal-only adaptation and space-time adaptation in the context of aerodynamics have been explored by Mani and Mavriplis (2007) and Flynt and Mavriplis (2012) respectively, and work with the compressible Navier-Stokes equations has been done for both static domains, by Luo and Fidkowski (2011), and deforming domains, by Kast and Fidkowski (2013).

3 One-dimensional shallow water equations

In one space dimension the shallow water equations take the form

$$h_t + (hu)_x = 0 \quad (3a)$$

$$(hu)_t + (hu^2 + \frac{1}{2}gh^2)_x = -ghB_x. \quad (3b)$$

Here, $u(x, t)$ is the depth-averaged velocity, $B(x)$ is the bottom surface elevation relative to mean sea level, g is the gravitational constant, and $h(x, t)$ is the fluid depth. We will use $\eta(x, t)$ to denote the water surface elevation,

$$\eta(x, t) = h(x, t) + B(x).$$

The shallow water equations are a special case of a hyperbolic system of equations,

$$q_t(x, t) + f(q)_x = \psi(q, x) \quad (4)$$

in one dimension and

$$q_t(x, y, t) + f(q)_x + g(q)_y = \psi(q, x, y) \quad (5)$$

in two dimensions, where q is a vector of unknowns, $f(q)$ and $g(q)$ are the vectors of corresponding fluxes, and ψ is a vector of source terms. These appear in the study of numerous physical phenomena where wave motion is important, and hence methods for numerically calculating solutions to these systems of partial differential equations have broad applications over multiple disciplines.

As mentioned above, when tracking a tsunami in the ocean the nonlinear shallow water equations essentially reduce to the linear shallow water equations. To linearize the shallow water equations about the ocean at rest, we begin by letting $\mu = hu$ represent the momentum and noting that the momentum equation from (3) can be rewritten as

$$\mu_t + (hu^2)_x + gh(h + B)_x = 0.$$

Linearizing this equation as well as the continuity equation about a flat surface $\bar{\eta}$ and zero velocity $\bar{u} = 0$, with $\bar{h}(x) = \bar{\eta} - B(x)$ gives

$$\tilde{\eta}_t + \tilde{\mu}_x = 0 \quad (6a)$$

$$\tilde{\mu}_t + g\bar{h}(x)\tilde{\eta}_x = 0 \quad (6b)$$

for the perturbation $(\tilde{\eta}, \tilde{\mu})$ about $(\bar{\eta}, 0)$. Dropping tildes and setting

$$A(x) = \begin{bmatrix} 0 & 1 \\ g\bar{h}(x) & 0 \end{bmatrix}, \quad q(x, t) = \begin{bmatrix} \eta \\ \mu \end{bmatrix}, \quad (7)$$

gives us the system

$$q_t(x, t) + A(x)q_x(x, t) = 0. \quad (8)$$

We now derive the adjoint equation for a linear hyperbolic system of partial differential equations of the form (8) posed on an interval $a \leq x \leq b$ and over a time interval $t_0 \leq t \leq t_f$, subject to some known initial conditions, $q(x, t_0)$, and some boundary conditions at $x = a$ and $x = b$. In the linearized shallow water case $A(x)$ and $q(x, t)$ are given by (7), although the analysis shown below applies more generally to any time dependent hyperbolic system of equations. In Section 2 we considered the case where we care about $J = \phi^T x$ where x was the solution to an algebraic system of equations, now suppose we are interested in calculating the value of a functional

$$J = \int_a^b \varphi^T(x) q(x, t_f) dx \quad (9)$$

for some given $\varphi(x)$. For example, if $\varphi(x) = \delta(x - x_0)$ then $J = q(x_0, t_f)$ is the solution value at the point $x = x_0$ at the final time t_f . This is the situation we consider in this paper, with the delta function smeared out around the region of interest for the computational approach.

If $\hat{q}(x, t)$ is any other appropriately sized vector of functions then multiplying this by (8) and integrating in both space and time yields

$$\int_a^b \int_{t_0}^{t_f} \hat{q}^T(x, t) (q_t(x, t) + A(x)q_x(x, t)) dx dt = 0 \quad (10)$$

for any time $t_0 < t_f$. Then integrating by parts in space and then in time yields the equation

$$\int_a^b \hat{q}^T q \Big|_{t_0}^{t_f} dx + \int_{t_0}^{t_f} \hat{q}^T A q \Big|_a^b dt - \int_{t_0}^{t_f} \int_a^b q^T \left(\hat{q}_t + (A^T \hat{q})_x \right) dx dt = 0. \quad (11)$$

By defining the adjoint equation,

$$\hat{q}_t(x, t) + (A^T(x) \hat{q}(x, t))_x = 0, \quad (12)$$

setting $\hat{q}(x, t_f) = \varphi(x)$, and selecting the appropriate boundary conditions for $\hat{q}(x, t)$ such that the integral in time vanishes (which varies based on the specific system being considered), we can eliminate all terms from (11) except the first term, to obtain

$$\int_a^b \hat{q}^T(x, t_f) q(x, t_f) dx = \int_a^b \hat{q}^T(x, t_0) q(x, t_0) dx. \quad (13)$$

Therefore, the integral of the inner product between \hat{q} and q at the final time is equal to the integral at the initial time t_0 :

$$J = \int_a^b \hat{q}^T(x, t_0) q(x, t_0) dx. \quad (14)$$

Note that we can replace t_0 in (10) with any t so long as $t_0 \leq t \leq t_f$, which would yield (14) with t_0 replaced by t . From this we observe that the locations where the magnitude of the inner product $\hat{q}(x, t)^T q(x, t)$ is large, for any t with $t_0 \leq t \leq t_f$, are the areas that will have a significant effect on the inner product J . These are the candidate areas for refinement at time t . To make use of this, we must first solve the adjoint equation (12) for $\hat{q}(x, t)$. Note, however, that this requires using “initial” data $\hat{q}(x, t_f)$, so the adjoint problem must be solved backward in time. In Section 4 we will discuss in more detail the manner in which this is done.

First, we present a one-dimensional example that illustrates how the waves from the forward and adjoint equations propagate and can be combined to identify the waves that will reach a point of interest. Viewing this first in one dimension has the advantage that we can easily view the full time-history of waves in the forward and adjoint equations together in single plots in the x - t plane. The figures presented in this section were computed using Clawpack on a very fine grid to generate illustrations, but the particular numerical method is immaterial here. We are not testing the adjoint approach to AMR since we do not perform any adaptive refinement in this case. In Section 5 below we will present numerical results using GeoClaw with adaptive refinement and further discuss the numerical methods used there.

As an example we use the one-dimensional linearized shallow water equations and its adjoint on the domain $0 \leq x \leq 400$ km. We choose simplified topography that is piecewise constant, with depth 4000 m for $50 \leq x \leq 400$ and shallower depth 200 m for $0 \leq x \leq 50$. The step discontinuity from deep ocean to “continental shelf” is chosen so that waves remain localized and the plots are easy to interpret. For the same reason we use reflecting boundary conditions at each boundary rather than a more realistic shore:

$$u(0, t) = 0, \quad u(400, t) = 0 \quad t \geq t_0.$$

As initial data for $q(x, t)$ we introduce a hump of stationary water with a height of 0.4 m centered 125 km off shore. Figure 1 shows the resulting waves interacting with the boundaries and the discontinuity in bathymetry, at the location indicated by the dashed line. As time progresses the hump splits into equal right-going and left-going waves heading out towards the ocean and towards the continental shelf, respectively. When the left-going wave encounters the continental shelf it splits into a reflected and a transmitted wave. When any waves, e.g. either the original right-going wave or the newly transmitted wave, encounter the wall on either side of the domain the waves are reflected back in the other direction. This interplay between reflection and transmission of the waves at the bathymetry discontinuity and the reflection of waves at the two boundaries leads to a complex wave pattern.

For the adjoint solution, suppose that we are interested in the accurate estimation of the surface elevation in the interval between 10 and 25 km offshore, perhaps because that is the location of gauges with which we wish to compare our results.

3.1 Single Point In Time

Initially suppose we are only interested in one particular time, say $t_f = 4200$ seconds. Setting $J = \int_{10}^{25} \eta(x, t_f) dx$, the problem then requires that

$$\varphi(x) = \begin{bmatrix} I(x) \\ 0 \end{bmatrix}, \quad (15)$$

where

$$I(x) = \begin{cases} 1 & \text{if } 10 < x < 25 \\ 0 & \text{otherwise.} \end{cases} \quad (16)$$

Define

$$\hat{q}(x, t_f) = \begin{bmatrix} \hat{\eta}(x, t_f) \\ \hat{u}(x, t_f) \end{bmatrix} = \varphi(x),$$

and note that (10) holds for this problem. If we define the adjoint problem by

$$\begin{aligned} \hat{q}_t + \left(A^T(x) \hat{q} \right)_x &= 0 & x \in [0, 400], \quad t_0 \leq t \leq t_f \\ \hat{u}(0, t) = 0, \quad \hat{u}(400, t) &= 0 & t_0 \leq t \leq t_f, \end{aligned}$$

then (13) holds, which is the expression that allows us to use the inner product of the adjoint and forward problems at each time step to determine what regions will influence the point of interest at the final time.

As the “initial” data for $\hat{q}(x, t_f) = \varphi(x)$ we have a square pulse in water height, which was described above in Equations (15) and (16) at the final time. As time progresses backwards, the pulse splits into equal left-going and right-going waves which interact with the walls and the bathymetry discontinuity giving both reflected and transmitted waves. Figure 1 also shows the results of solving this adjoint problem.

To better visualize how the waves are moving through the domain, it is helpful to look at the data in the x - t plane as shown in Figure 2. For Figure 2, the

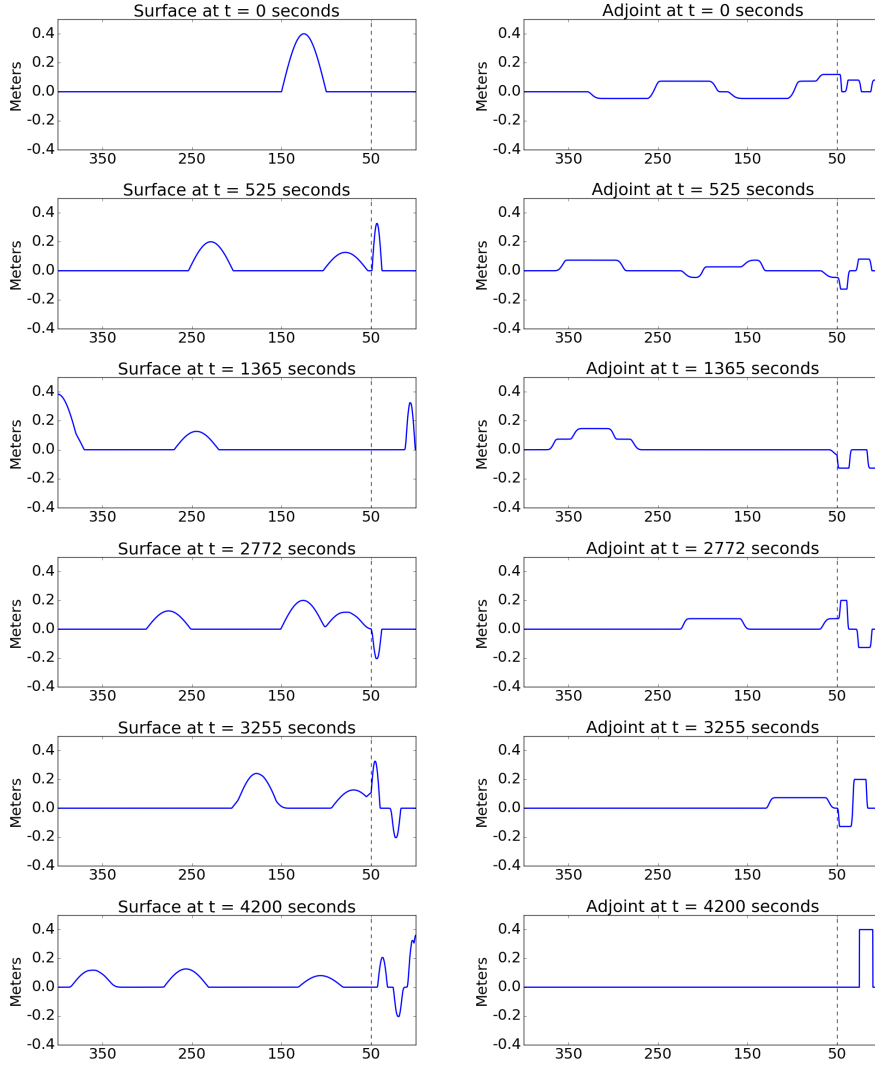


Fig. 1 An idealized tsunami interacting with a step discontinuity in bathymetry, for both the forward and the adjoint problems. The dashed line indicated the location of the discontinuity, 50 km offshore.

horizontal axis is the position, x , and the vertical axis is time. The left plot shows in red the locations where the magnitude of height of the tsunami in the forward problem is greater than or equal to 0.1 meters above mean sea level. On the right side of Figure 2 we show the adjoint solution that is computed starting with the square wave data at the final time t_f , indicating in blue the regions where the first component $\hat{\eta}$ is greater than or equal to 0.1.

On the left side of Figure 3 we have overlayed the magnitudes of the water heights for the forward and adjoint solutions, and viewing the data in the x - t

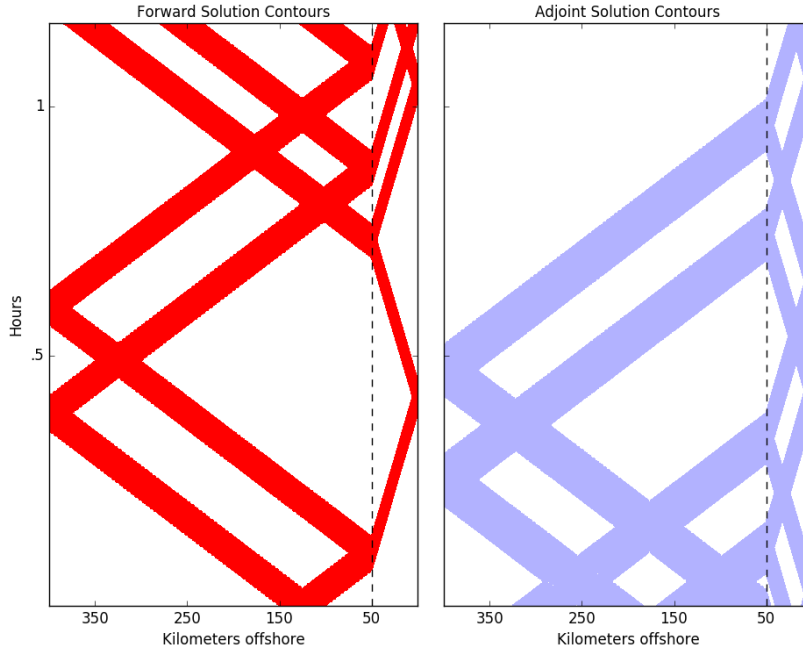


Fig. 2 On the left, the locations where the magnitude of the surface elevation η in the forward problem is greater than or equal to 0.1 meters above mean sea level are shown in red. On the right, the locations where the magnitude of $\hat{\eta}$ in the adjoint solution is greater than or equal to 0.1 are shown in blue. The time axis is the same for both plots.

plane makes it fairly clear which parts of the wave from the forward solution actually effect our region of interest at the final time.

Figure 3 also shows, in green on the right, the locations where the magnitude of the inner product between the forward and adjoint solution is greater than or equal to 0.1 as time progresses. At each time step this is clearly identifying the regions in the computational domain that will affect our region of interest at the final time. If we were using adaptive mesh refinement, these areas, identified by where the magnitude of $\hat{q}^T(x,t)q(x,t)$ exceeds some tolerance, are the areas we should consider for adaptive refinement. Note that a mesh refinement strategy based only on the areas where the magnitude of $\eta(x,t)$ is large would result in refinement of many areas in the computational domain that will have no effect on our area of interest at the final time (all the red regions in the left plot of Figure 3).

It is important to note that in the left side of Figure 3 there are places where red and blue waves overlap that do not show up in the plot on the right side. These are areas where a wave moving in one direction in the forward solution crosses a wave moving in the other direction in the adjoint solution. Even though both $q(x,t)$ and $\hat{q}(x,t)$ are nonzero vectors in these regions, the inner product of the two is equal to zero. This is easily verified by computing the eigenvectors of the coefficient matrices A and A^T defining the hyperbolic problems for q and \hat{q} (see, for example LeVeque (2002)). The eigenvectors of A are $[1, \pm c]^T$, where $c = \sqrt{gh}$

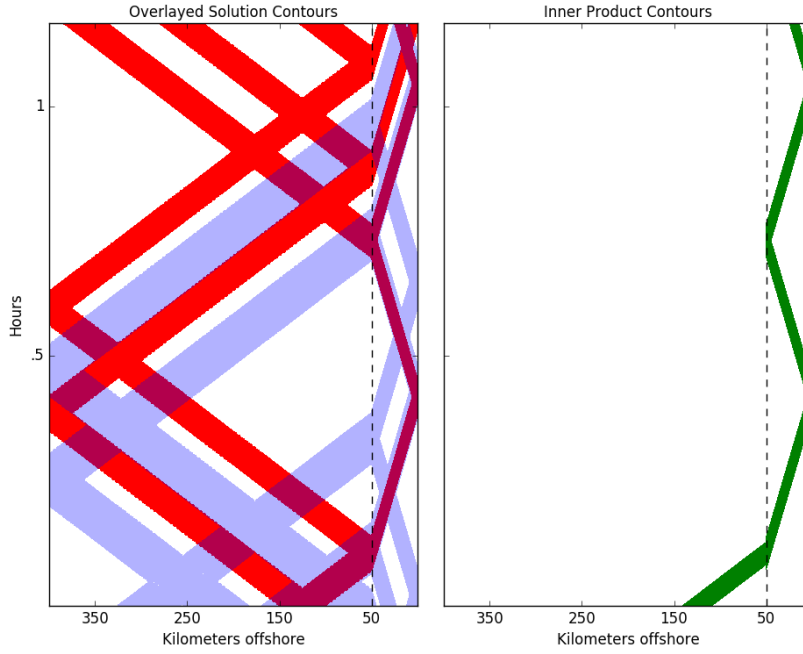


Fig. 3 The plots of the magnitudes of η and $\hat{\eta}$ from Figure 2 are overlaid in the left figure. The region where the inner product of the two vectors $q(x, t)$ and $\hat{q}(x, t)$ is above a threshold is shown on the right, picking out only the wave that reaches the target location at $10 \leq x \leq 25$ the final time. The time axis is the same for both plots.

is the wave speed. Hence the solution q in a purely left-going wave is proportional to the vector $[1, -c]^T$, while in a purely right-going wave is proportional to $[1, +c]^T$. The eigenvectors of A^T , on the other hand, are $[\pm c, 1]^T$ and each of these is orthogonal to one of the eigenvectors of A (and hence the inner product is zero for crossing waves). It is only when the waves are aligned on the left side of Figure 3 that the inner product is seen to be nonzero on the right side of the figure. This further illustrates the power of the adjoint approach to identify only the waves that will reach the target location.

3.2 Time Range

In practice we are rarely interested in the tsunami amplitude at some location at only a single time, we are more likely to be interested in the solution over some time range, often over the entire simulation time. But note that once we have computed the adjoint solution going backward from time t_f , we immediately know the adjoint solution starting at some earlier time $\bar{t} < t_f$: it is simply the same solution translated earlier in time by $t_f - \bar{t}$, since the linearized adjoint equation is autonomous in time. The formulas will be made more precise in the next section, but in terms of Figure 3 we can think of moving the data for the adjoint to an earlier time as simply translating the blue solution in the left figure downward by

this time increment. Figure 4 illustrates the result if we consider setting \bar{t} to all possible values between $t_s = 3800$ seconds and $t_f = 4200$ seconds. The small blue rectangle in the top corner of this plot shows the region in space-time that we are now concentrating on as our target space-time region, and the green portions in the figure on the right of Figure 4 show where the inner product of the forward solution and any of these translated adjoint solutions is above the threshold of 0.1. We clearly see that, relative to Figure 3, there is an additional wave that must be tracked since it arrives at the target spatial region during the target time period.

If we were interested in any wave that can arrive in the target region over the full simulation time $0 \leq t \leq t_f$, then we would extend this by looking at all possible downward translates of the adjoint solution. In this particular example, this would not identify any additional waves beyond those already found, since the other waves would not arrive at the target location until times beyond t_f .

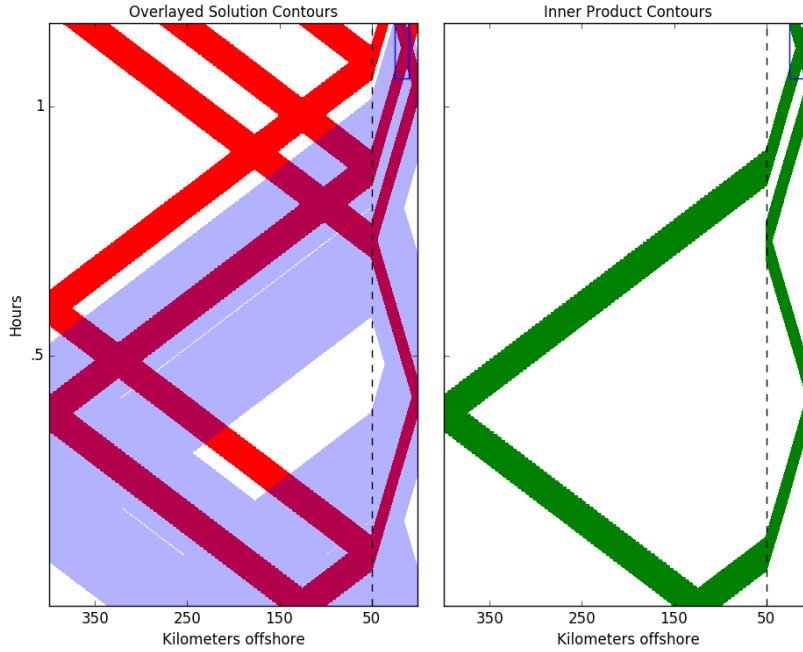


Fig. 4 Computed results for one-dimensional shallow water equations in the case when the solution $q(x, t)$ is desired at the target location $10 \leq x \leq 25$ km over a time interval from 3800 to 4200 seconds, as indicated by the box in each $x-t$ plot. Left: Plots showing $\eta(x, t)$ and the adjoint solutions $\hat{\eta}(x, \tau)$ for shifted values of τ as described in the text. Right: Regions where the maximum inner product over the given time range exceeds the threshold, showing the additional wave that reaches the target region relative to the case shown in Figure 3. The time axis is the same for both plots.

4 Combining mesh refinement and the adjoint problem

We now discuss in more detail how the adjoint solution might be used in guiding adaptive mesh refinement, still focusing on the one-dimensional case presented above.

Before solving the forward problem, we would first solve the adjoint equation (12) backward in time. Since GeoClaw and other numerical software is designed to solve equations forward in time, we consider the function

$$\tilde{q}(x, t) = \hat{q}(x, t_f - t).$$

This gives us the new problem

$$\begin{aligned} \tilde{q}_t - \left(A^T(x) \tilde{q} \right)_x &= 0 & x \in [a, b], \quad t > 0 \\ \tilde{q}(a, t) &= \hat{q}(a, t_f - t) & 0 \leq t \leq t_f - t_0 \\ \tilde{q}(b, t) &= \hat{q}(b, t_f - t) & 0 \leq t \leq t_f - t_0 \end{aligned}$$

with initial condition $\tilde{q}(x, 0) = \varphi(x)$. This problem is then solved forward in time. Snapshots of this solution are saved at regular time intervals, t_0, t_1, \dots, t_N , from which snapshots of the adjoint solution are retrieved by simply setting

$$\hat{q}(x, t - t_n) = \tilde{q}(x, t_n)$$

for $n = 0, 1, \dots, N$.

With the adjoint solution in hand, we now turn to the forward problem. In our approach to GeoClaw, described more fully in the two-dimensional case in Section 5, we solve the adjoint equation on a fixed spatial resolution and output at discrete times. To flag cells for refinement as we now solve the forward problem, we will generally need to estimate the adjoint solution on finer grids in both space and time. To address this issue, the solution for the adjoint problem at the necessary spatial locations is approximated using linear (or bilinear in 2D) interpolation from the data present on the coarser grid defined by the snapshots.

4.1 Single Point In Time

If we are interested in the solution of the forward problem at our target area only at the final time, then when solving the forward problem we take the inner product between the current time step in the forward problem and the time step in the adjoint problem in order to determine which areas in the forward wave are going to impact the region of interest. When considering the forward problem at time t that lies between two snapshot times of the adjoint, say

$$t_n \leq t \leq t_{n+1},$$

both $\hat{q}(x, t_n)$ and $\hat{q}(x, t_{n+1})$ are taken into account. Rather than interpolating in time, since we wish to refine any parts of the domain that will have a significant impact on the final solution, we take a more conservative approach and refine wherever the magnitude of the inner product

$$\max_{\tau=t_n, t_{n+1}} \left| \hat{q}^T(x, \tau) q(x, t) \right| \quad (17)$$

is above some tolerance. Note that we must save snapshots of the adjoint at sufficiently dense output times for this to be sufficient. These areas are then flagged for refinement, and the next time step is taken.

4.2 Time Range

Suppose that we are instead interested in the accurate estimation of the forward problem in same location for some time range $t_s \leq t \leq t_f$, where $t_0 \leq t_s \leq t_f$. Define $\hat{q}(x, t; \hat{t})$ as the adjoint based on data $\hat{q}(x, \hat{t}) = \varphi(x)$. Then for each \hat{t} in the interval $[t_s, t_f]$, we need to consider the inner product of $q(x, t)$ with $\hat{q}(x, t; \hat{t})$. Note that since the adjoint is autonomous in time, $\hat{q}(x, t; \hat{t}) = \hat{q}(x, t_f - \hat{t} + t; t_f)$. Therefore, we must consider the inner product

$$\hat{q}^T(x, t_f - \hat{t} + t; t_f)q(x, t)$$

for $\hat{t} \in [t_s, t_f]$. Since we are in fact only concerned when the magnitude of this inner product is greater than some tolerance, we can simply consider

$$\max_{t_s \leq \hat{t} \leq t_f} \left| \hat{q}^T(x, t_f - \hat{t} + t; t_f)q(x, t) \right|$$

and refine when this maximum is above the given tolerance. Define $\tau = t_f - \hat{t} + t$. Then this maximum can be rewritten as

$$\max_{T \leq \tau \leq t} \left| \hat{q}^T(x, \tau; t_f)q(x, t) \right| \quad (18)$$

where $T = \min(t + t_f - t_s, t_f)$.

We now drop the cumbersome notation $\hat{q}(x, t; t_f)$ in favor of the simpler $\hat{q}(x, t)$ with the understanding that the adjoint is based on the data $\hat{q}(x, t_f) = \varphi(x)$. Note that we still only need to solve one adjoint problem in this case, we simply use it over a larger time range in evaluating (18) than in (17).

5 Two-dimensional shallow water equations

In two space dimension the shallow water equations take the form

$$h_t + (hu)_x + (hv)_y = 0 \quad (19a)$$

$$(hu)_t + (hu^2 + \frac{1}{2}gh^2)_x + (huv)_y = -ghB_x \quad (19b)$$

$$(hv)_t + (huv)_x + (hv^2 + \frac{1}{2}gh^2)_y = -ghB_y. \quad (19c)$$

Here, $u(x, y, t)$ and $v(x, y, t)$ are the depth-averaged velocities in the two horizontal directions and $B(x, y)$ is the bottom surface elevation relative to mean sea level. Now the water surface elevation is given by

$$\eta(x, y, t) = h(x, y, t) + B(x, y).$$

Linearizing these equations about an ocean at rest, similar to what was done in Section 3 for the one dimensional case, gives

$$\begin{aligned}\tilde{\eta}_t + \tilde{\mu}_x + \tilde{\gamma}_y &= 0 \\ \tilde{\mu}_t + g\bar{h}(x, y)\tilde{\eta}_x &= 0 \\ \tilde{\gamma}_t + g\bar{h}(x, y)\tilde{\eta}_y &= 0\end{aligned}$$

for the perturbation $(\tilde{\eta}, \tilde{\mu}, \tilde{\gamma})$ about $(\bar{\eta}, 0, 0)$. Dropping tildes and setting

$$A_1(x, y) = \begin{bmatrix} 0 & 1 & 0 \\ g\bar{h}(x, y) & 0 & 0 \\ 0 & 0 & 0 \end{bmatrix}, \quad A_2(x, y) = \begin{bmatrix} 0 & 0 & 1 \\ 0 & 0 & 0 \\ g\bar{h}(x, y) & 0 & 0 \end{bmatrix}, \quad q(x, y, t) = \begin{bmatrix} \eta \\ \mu \\ \gamma \end{bmatrix},$$

gives us the system

$$q_t(x, y, t) + A_1(x, y)q_x(x, y, t) + A_2(x, y)q_y(x, y, t) = 0. \quad (20)$$

For a general system of the form (20) we now derive the adjoint equation posed on an interval $a \leq x \leq b$, $\alpha \leq y \leq \beta$ and over a time interval $t_0 \leq t \leq t_f$, subject to some known initial conditions $q(x, y, t_0)$ and some boundary conditions at $x = a$, $x = b$, $y = \alpha$ and $y = \beta$. If $\hat{q}(x, y, t)$ is an appropriately sized vector of functions then note that

$$\int_{t_0}^{t_f} \int_a^b \int_\alpha^\beta \hat{q}^T (q_t + A_1(x, y)q_x + A_2(x, y)q_y) dy dx dt = 0.$$

Following the same basic steps we used in one dimension to go from (10) to (11), integrating by parts yields the equation

$$\begin{aligned}\int_a^b \int_\alpha^\beta \hat{q}^T q|_{t_0}^{t_f} dy dx + \int_{t_0}^{t_f} \int_\alpha^\beta \hat{q}^T A_1(x, y)q|_a^b dy dt + \int_{t_0}^{t_f} \int_a^b \hat{q}^T A_2(x, y)q|_\alpha^\beta dx dt \\ - \int_{t_0}^{t_f} \int_a^b \int_\alpha^\beta q^T \left(\hat{q}_t + \left(A_1^T(x, y)\hat{q} \right)_x + \left(A_2^T(x, y)\hat{q} \right)_y \right) dy dx dt = 0,\end{aligned} \quad (21)$$

and if we can define an adjoint problem such that all but the first term in this equation vanishes then we are left with

$$\int_a^b \int_\alpha^\beta \hat{q}^T(x, y, t_f)q(x, y, t_f) dy dx = \int_a^b \int_\alpha^\beta \hat{q}^T(x, y, t_0)q(x, y, t_0) dy dx, \quad (22)$$

which is the expression that allows us to use the inner product of the adjoint and forward problems at each time step to determine what regions will influence the point of interest at the final time.

This requires that the adjoint equation have the form

$$\hat{q}_t + \left(A_1^T(x, y)\hat{q} \right)_x + \left(A_2^T(x, y)\hat{q} \right)_y = 0 \quad (23)$$

over the same domain as the forward problem. The correct boundary conditions to use are zero normal velocity at all interfaces between any wet cell and dry cell so that the boundary terms also drop out of expression (21) to obtain (22).

6 GeoClaw Tsunami Modeling Example

Finally, we present a tsunami propagation example utilizing the adjoint method to guide adaptive mesh refinement, as implemented in the GeoClaw software package. In principle the adjoint flagging methodology could be used in conjunction with other tsunami models, although we know of no other open source software that provides similar adaptive mesh refinement capabilities. Verification of the results is performed by comparing the results from the adjoint method approach to the default approach already present in the GeoClaw software. The algorithms used in GeoClaw for tsunami modeling are described in detail in LeVeque et al (2011), and only a brief introduction will be given here. In general, GeoClaw solves the two-dimensional nonlinear shallow water equations in the form of a nonlinear system of hyperbolic conservation laws for depth and momentum. The numerical methods used are high-resolution Godunov-type finite volume methods, in which the discrete solution is given by cell averages of depth and momentum over the grid cells and the solution is updated in each time step based on fluxes computed at the cell edges. In Godunov-type methods, these fluxes are determined by solving a “Riemann problem” at each cell edge, which consists of the hyperbolic problem with piecewise constant initial data given by the adjacent cell averages. The general theory of these methods is presented in LeVeque (2002), for example, and details of the Riemann solver in GeoClaw can be found in George (2008). Away from coastlines, this solver reduces to a Roe solver for the shallow water equations plus bathymetry, which means that the eigenstructure of a locally linearized Riemann problem is solved at each cell interface, making it no more expensive in the deep ocean than simply solving the linearized equations, but also capable of robustly handling nonlinearity near shore and inundation.

As an example, we consider a tsunami generated by a hypothetical earthquake on the Alaska-Aleutian subduction zone, the event denoted AASZe04 in the probabilistic hazard study of Crescent City, CA performed by González et al (2014). The major waves impinging on Crescent City from this hypothetical tsunami all occurred within 11 hours after the earthquake, so simulations will be run to this time. To simulate the effects of this tsunami on Crescent City a coarse grid is used over the entire Pacific (1 degree resolution) where the ocean is at rest. In addition to AMR being used to track propagating waves on finer grids, higher levels of refinement are allowed or enforced around Crescent City when the tsunami arrives. A total of 4 levels of refinement are used, starting with 1-degree resolution on the coarsest level, and with refinement ratios of 5, 6, and 6 from one level to the next. Only 3 levels were allowed over most of the Pacific, and the remaining level was used over the region around Crescent City. Level 4, with 20-second resolution, is still too coarse to provide any real detail on the effect of the tsunami on the harbor. It does, however, allow for a comparison of flagging cells for refinement using the adjoint method and using the default method implemented in Geoclaw. In this simulation we used 1 arc-minute bathymetry from the ETOPO1 Global Relief Model of Amante, C and Eakins, BW (2009) for the entire simulation area, as well as 1 arc-second and 1/3 arc-second bathymetry over the region about Crescent City from Grothe et al (2011). Internally, GeoClaw constructs a piecewise-bilinear function from the union of any provided topography files. This function is then integrated over computational grid cells to obtain a single cell-averaged topography value in each grid cell in a manner that is consistent between refinement levels.

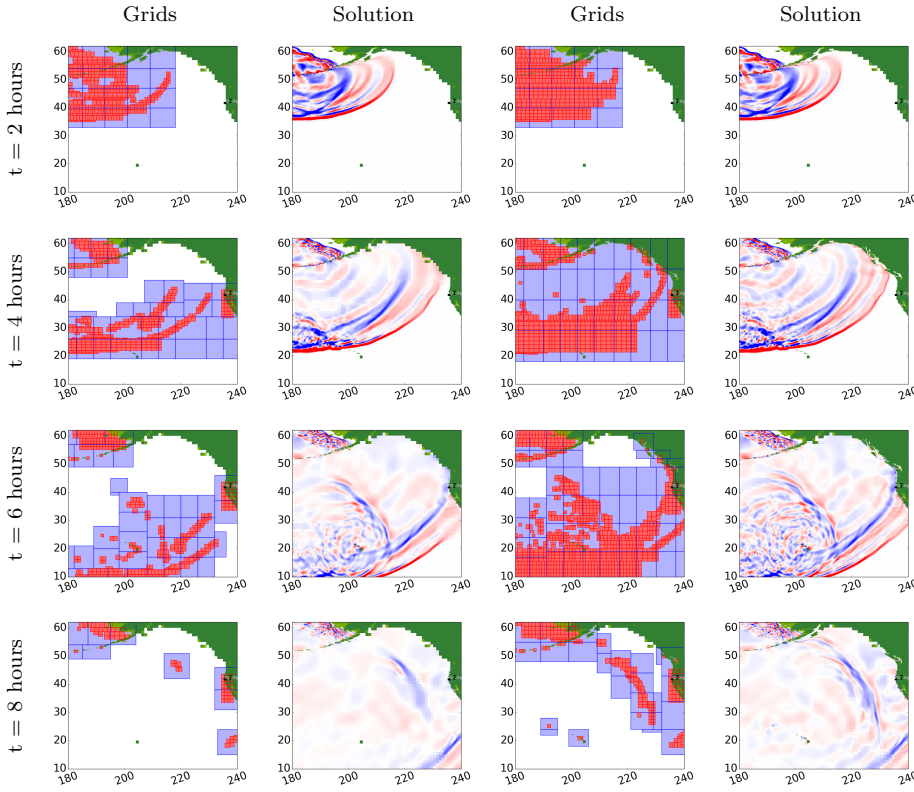


Fig. 5 Computed results for tsunami propagation problem on two different runs utilizing the surface-flagging technique. The x -axis and y -axis are latitude and longitude, respectively. The grids and solution along the left correspond to the simulation with a tolerance of 0.14, and the grids and solution along the right correspond to the simulation with a tolerance of 0.09. In the grid figures each color corresponds to a different level of refinement: white for the coarsest level, blue for level two, and red for level three. The color scale for the solution figures goes from blue to red, and ranges between -0.3 and 0.3 meters (surface elevation relative to sea level). Times are in hours after the earthquake.

The default Geoclaw refinement technique flags cells for refinement when the elevation of the sea surface relative to sea level is above some set tolerance, as described in LeVeque et al (2011), where the adaptive refinement and time stepping algorithms are described in more detail. We will refer to this flagging method as surface-flagging. The value selected for this tolerance has a significant impact in the results calculated by the simulation, since a smaller tolerance will result in more cells being flagged for refinement. Consequently, a smaller tolerance both increases the simulation time required and theoretically increases the accuracy of the results.

Two Geoclaw simulations were performed using surface-flagging, one with a tolerance of 0.14 and another with a tolerance of 0.09. Figure 5 shows the results of these two simulations, along with the grids at different levels of refinement used, for the sake of comparison. Note that each grid outlined in the figure, colored based on its level of refinement, is a collection of cells at a particular refinement.

The grids and solution along the left of the figure correspond to the simulation with a tolerance of 0.14, and the grids and solution along the right of the figure correspond to the simulation with a tolerance of 0.09. Note that the simulation with a surface-flagging tolerance of 0.14 continues to refine the first wave until it arrives at Crescent City about 5 hours after the earthquake, but after about 6 hours stops refining the main secondary wave which reflects off the Northwestern Hawaiian (Leeward) Island chain before heading towards Crescent City. The second simulation, with a surface-flagging tolerance of 0.09 continues to refine this secondary wave until it arrives at Crescent City.

These two tolerances were selected because they are illustrative of two constraints that typically drive a Geoclaw simulation. The larger surface-flagging tolerance, of 0.14 was found to be approximately the largest tolerance that will refine the initial wave until it reaches Crescent City. Therefore, it essentially corresponds to a lower limit on the time required by the standard surface-flagging approach: any Geoclaw simulation with a larger surface-flagging tolerance would run more quickly but would fail to give accurate results for even the first wave. Note that for this particular example, even when the simulation will only give accurate results for the first wave to reach Crescent City, a large area of the wave front that is not headed directly towards Crescent City is being refined with the AMR. The smaller surface-flagging tolerance, of 0.09, refines all of the waves of interest that impinge on Crescent City thereby giving more accurate results at the expense of longer computational time, particularly since it also refines waves that will never reach Crescent City.

Now we consider the adjoint approach, which will allow us to refine only those sections of the wave that will affect our target region. For this example, we are interested in the accurate calculation of the water surface height in the area about Crescent City, California. To focus on this area, we define a circle of radius 1° centered about $(x_c, y_c) = (235.80917, 41.74111)$ where x and y are being measured in degrees. Setting

$$J = \int_{x_{min}}^{x_{max}} \int_{y_{min}(x)}^{y_{max}(x)} \eta(x, y, t_f) dy dx,$$

where the limits of integration define the appropriate circle, the problem then requires that

$$\varphi(x, y) = \begin{bmatrix} I(x, y) \\ 0 \\ 0 \end{bmatrix}, \quad (24)$$

where

$$I(x, y) = \begin{cases} 1 & \text{if } \sqrt{(x - x_c)^2 + (y - y_c)^2} \leq 1, \\ 0 & \text{otherwise.} \end{cases} \quad (25)$$

This function $\varphi(x, y)$ defines the “initial data” $\hat{q}(x, y, t_f)$ for the adjoint problem. Figure 6 shows the results for the simulation of this adjoint problem. For this simulation a grid with 15 arcminute = 0.25° resolution was used over the entire Pacific and no grid refinement was allowed. The simulation was run out to 11 hours.

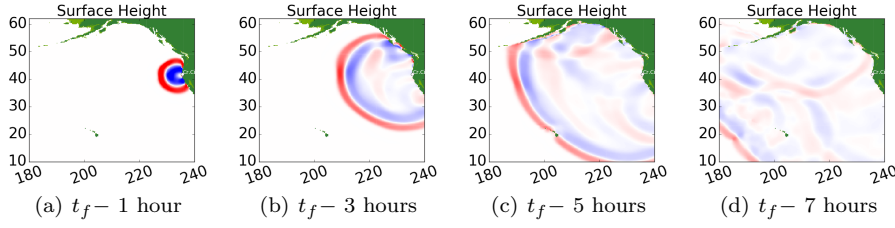


Fig. 6 Computed results for tsunami propagation adjoint problem. Times shown are the number of hours before the final time, since the “initial” conditions are given at the final time. The color scale goes from blue to red, and ranges between -0.05 and 0.05 .

The topography files used for the adjoint problem are the same as those used for the forward problem. However, given that the adjoint problem is being solved on a coarser grid than the forward problem, the coastline between the two simulations varies. Since the coastline varies between the two simulations, when computing the inner product it is possible to find grid cells that are wet in the forward solution and dry in the adjoint solution. In this case, the inner product in those grid cells is set to zero.

The simulation of this tsunami using adjoint-flagging for the AMR was run using the same initial grid over the Pacific, the same refinement ratios, and the same initial water displacement as our previous surface-flagging simulations. The only difference between this simulation and the previous one is the flagging technique utilized. The first waves arrive at Crescent City around 4 hours after the earthquake, so we set $t_s = 3.5$ hours and $t_f = 11$ hours. Recall that the areas where the maximum magnitude of the inner product over the appropriate time range,

$$\max_{T \leq \tau \leq t} \left| \hat{q}^T(x, y, \tau) q(x, y, t) \right|$$

with $T = \min(t + t_f - t_s, 0)$, is large are the areas where adaptive mesh refinement should take place.

Figure 7 shows the Geoclaw results for the surface height at various different times, along with the grids at different levels of refinement that were used and the maximum inner product in the appropriate time range. Compare this figure to Figure 5, noting the extent of the grids at each refinement level for each of the three simulations.

6.1 Computational Performance

The above example was run on a quad-core laptop, for both the surface-flagging and adjoint-flagging methods, and the OpenMP option of GeoClaw was enabled which allowed all four cores to be utilized. The timing results for the tsunami simulations are shown in Table 1. Recall that two simulations were run using surface-flagging, one with a tolerance of 0.14 (“Large Tolerance” in the table) and another with a tolerance of 0.09 (“Small Tolerance” in the table). Finally, a GeoClaw example using adjoint-flagging was run with a tolerance of 0.004 (“Forward”

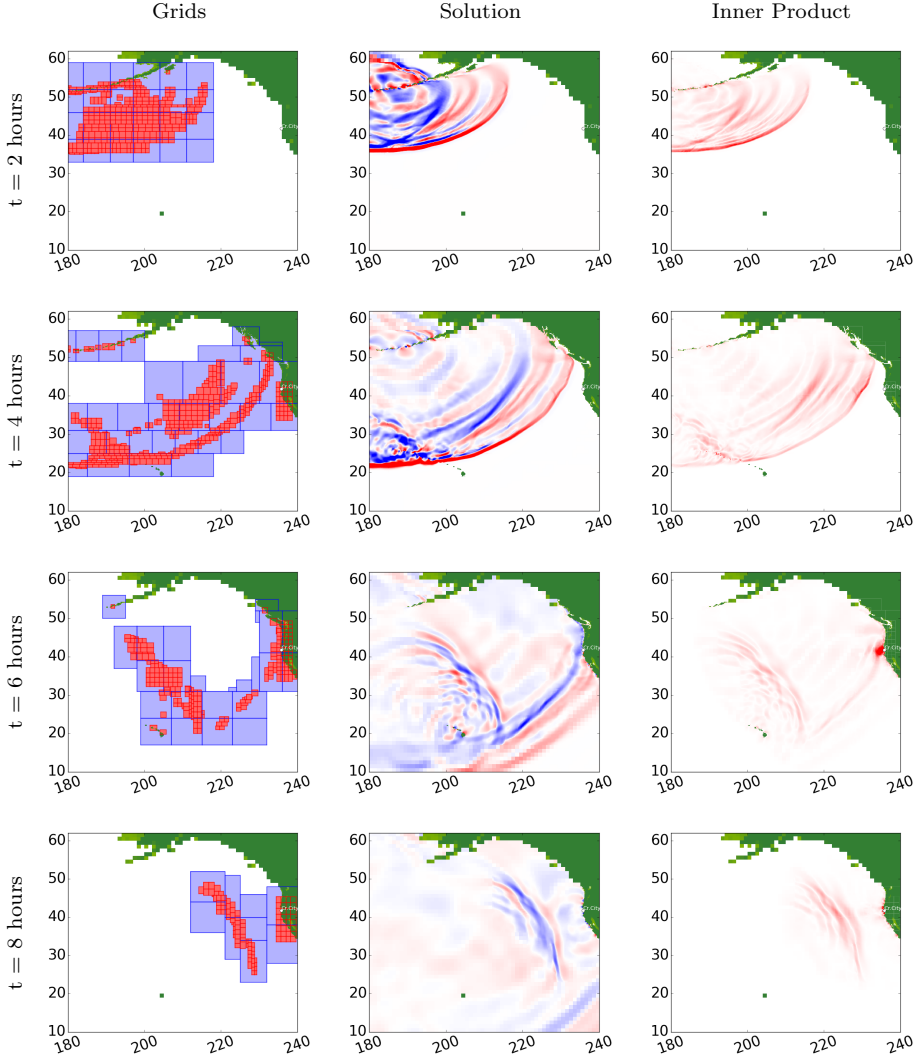


Fig. 7 Computed results for tsunami propagation problem when adjoint-flagging is used. The x -axis and y -axis are latitude and longitude, respectively. In the grid figures each color corresponds to a different level of refinement: white for the coarsest level, blue for level two, and red for level three. The color scale for the surface height figures goes from blue to red, and ranges between -0.3 and 0.3 . The color scale for the inner product figures goes from white to red, and ranges between 0 and 0.04 . Times are in hours since the earthquake.

in the table), which of course required a simulation of the adjoint problem the timing for which is also shown in the table.

As expected, between the two GeoClaw simulations which utilized surface-flagging the one with the larger tolerance took significantly less time. Note that although solving the problem using adjoint-flagging did require two different simulations, the adjoint problem and the forward problem, the computational time required is only slightly more than the timing required for the large tolerance

surface-flagging case. Another consideration when comparing the adjoint-flagging

Table 1 Timing comparison for the example in Section 6.1 given in seconds.

Surface-Flagging		Adjoint-Flagging	
Small Tolerance	Large Tolerance	Forward	Adjoint
8310	5724	5984	27

method with the surface-flagging method already in place in GeoClaw is the accuracy of the results. To test this, gauges were placed in the example and the output at the gauges compared across the two different methods.

For the tsunami example two gauges are used: gauge 1 is placed at $(x, y) = (235.536, 41.67)$ which is on the continental shelf to the west of Crescent City, and gauge 2 is placed at $(x, y) = (235.80917, 41.74111)$ which is in the harbor of Crescent City. In Figure 8 the gauge results from the adjoint method are shown in blue, the results from the surface-flagging technique with a tolerance of 0.14 are shown in red, and the results from the surface-flagging technique with a tolerance of 0.09 are shown in green. Note that the blue and green lines are in fairly good agreement, indicating that the use of the adjoint method achieved a comparable accuracy with the smaller tolerance run using the surface-flagging method, although the time required was significantly less. While the larger tolerance run using the surface-flagging method had a similar time requirement to the adjoint method simulation, it agrees fairly well only for the first wave but then rapidly loses accuracy.

7 Conclusions

In this paper, we first presented the adjoint methodology in some detail in hopes that it will also be useful in other tsunami modeling software in the future, and perhaps in other contexts for exploring sensitivities.

Integrating the adjoint method approach to cell flagging into the already existing AMR algorithm in GeoClaw results in significant time savings for the tsunami simulation shown in this work. For the tsunami example we examined here, the surface-flagging simulation with a tolerance of 0.14 has the advantage of a low computational time but only provides accurate results for the first wave to reach Crescent City. The surface-flagging simulation with a tolerance of 0.09 refines more waves and therefore provides accurate results for a longer period of time. However, it has the disadvantage of having a long computational time requirement since it refines in many regions where the waves are not important to the modeling of Crescent City. The use of the adjoint method allows us to retain accurate results while also reducing the computational time required. Equally, or perhaps even more importantly, the adjoint approach gives more confidence that the appropriate waves have been refined to capture the tsunami impact at the target location than *ad hoc* attempts to guide the refinement regions manually.

The code for all the examples presented in this work is available online at Davis (2015), and includes the code for solving the adjoint Riemann problems.

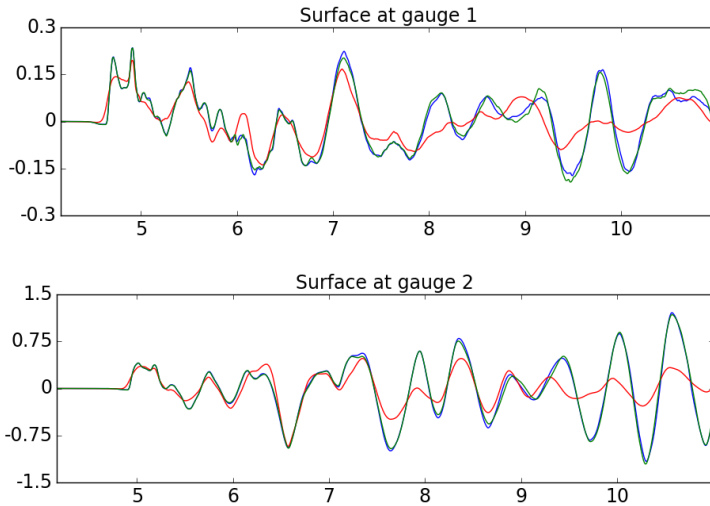


Fig. 8 Computed results at gauges for tsunami propagation problem. The results from the simulation using the adjoint method are shown in blue, the results from the simulation using the surface-flagging method with a tolerance of 0.14 are shown in red, and the results from the simulation using the surface-flagging method with a tolerance of 0.09 are shown in green. Along the x -axis, the time since the occurrence of the earthquake is shown in hours.

This code can be easily modified to solve other tsunami modeling problems. This repository also contains other examples illustrating how adjoint flagging can be used with AMRClaw, the more general adaptive refinement code in Clawpack for general hyperbolic systems. Another example of the adjoint method being used in GeoClaw for tsunami modeling can be found in Borrero et al (2015).

8 Additional Comments and Future Work

The method described in this paper flags cells for refinement wherever the magnitude of the relevant inner product between the forward and adjoint solutions is above some tolerance. Choosing a sufficiently small tolerance will trigger refinement of all regions where the forward solution might need to be refined, and in our current approach these will be refined to the finest level specified in the computation for refinement in the ocean (finer levels may be imposed near the target location). We believe this approach is already a significant advance over the method currently used in GeoClaw for many trans-oceanic modeling problems. Although a tolerance must be chosen in order to define the cutoff for flagging cells based on the inner product, this is similar to the current need for setting a tolerance on the surface elevation for flagging cells, and has the great advantage that it identifies the waves that will reach the target location rather than potentially refining everywhere there are waves.

We will also continue to explore ways to better optimize efficiency — it would be desirable to have error bounds based on the adjoint solution that could be used to refine the grid more selectively to achieve some target error tolerance for the final quantity of interest. For some problems we believe this can be accomplished

using the Richardson extrapolation error estimator that is built into AMRClaw to estimate the point-wise error in the forward solution and then using the adjoint solution to estimate its effect on the final quantity of interest. This is currently under investigation and we hope to develop a robust strategy that can be applied to a wide variety of problems for general inclusion into Clawpack. However, there are potential difficulties in deriving more precise error estimation via the adjoint method for use in GeoClaw. The functional $J(q)$ that we have defined, e.g. by integrating the solution against the piecewise constant function over a one degree square around Crescent City defined by (25), is not exactly the quantity we are trying to compute in the end. Rather we wish to compute the time history at one or more particular gauge locations (as shown in Figure 8) or the detailed inundation in the community. The functional $J(q)$ is simply designed to radiate waves from the Crescent City vicinity in order to determine what waves in the forward problem are important to track. The error in some true quantity of interest such as the maximum flooding depth may vary from point to point in the community. For this reason more research is required to investigate the extent to which error estimates on $J(q)$ can be employed in practice. Another potential difficulty is that the bathymetry $B(x, y)$ is not at all smooth at the grid resolution typically needed to model trans-ocean wave propagation. Because the wave length of tsunamis is so long, good accuracy is often observed in spite of this (as found in many validation studies of GeoClaw and other tsunami software based on the shallow water equations). However, this may limit the applicability of Richardson extrapolation error estimation.

Using adaptive refinement in solving the adjoint equation may also be desirable. In this paper the adjoint solution was computed on a fixed grid. Allowing AMR to take place when solving the adjoint equation could increase the accuracy of the results, since it would enable a more accurate (while still efficient) evaluation of the inner product between the forward and adjoint solutions. In an effort to guide the AMR of the adjoint problem in a similar manner to the method used for the forward problem, the two problems would need to be solved somewhat in conjunction and the inner product between the two considered for both the flagging of the cells in the adjoint problem as well as the flagging of cells in the forward problem. One approach that is used to tackle this issue is checkpointing, where the forward problem is solved and the solution at a small number of time steps is stored for use when solving the adjoint problem, as seen for example in Wang et al (2009). The automation of this process is another area of future work, and involves developing an evaluation technique for determining the number of checkpoints to save or when to shift from refining the adjoint solution to refining the forward solution and vice versa.

For the tsunami example presented here we linearized the shallow water equations about the ocean at rest, and the adjoint equations then have essentially the same form. This is sufficient for many important applications, in particular for tsunami applications where the goal is to track waves in the ocean where the linearization is essentially independent of the forward solution. If an adjoint method is desired in the inundation zone, or for other nonlinear hyperbolic equations, then the adjoint equation is derived by linearizing about a particular forward solution. This would again require the development of an automated process to shift between solving the forward problem, linearizing about that forward problem, and solving the corresponding adjoint problem. Finally, in this work we assumed wall

boundary conditions when a wave interacted with the coastline in the adjoint problem. This assumption, along with the use of the linearized shallow water equations, becomes significant when a wave approaches a shore line. Allowing for more accurate interactions between waves and the coastline in the solution of the adjoint problem is another area for future work.

References

- Akcelik V, Biros G, Ghattas O (2002) Parallel multiscale Gauss-Newton-Krylov methods for inverse wave propagation. In: Proceedings of the 2002 ACM/IEEE Conference on Supercomputing, SC '02, pp 1–15
- Amante, C and Eakins, BW (2009) ETOPO1 1 Arc-Minute Global Relief Model: Procedures, Data Sources and Analysis. NOAA Technical Memorandum NES-Dis NGDC-24, National Geophysical Data Center, NOAA, DOI 10.7289/V5C8276M
- Asner L, Tavener S, Kay D (2012) Adjoint-based a posteriori error estimation for coupled time-dependent systems. *SIAM J Sci Comput* 34:A2394A2419
- Becker R, Rannacher R (2001) An optimal control approach to a posteriori error estimation in finite element methods. *Acta Numerica* 10:1–102
- Berger M, Rigoutsos I (1991) An algorithm for point clustering and grid generation. *IEEE T Syst Man Cyb* 21(5):1278–1286
- Berger MJ, George DL, LeVeque RJ, Mandli KT (2011) The geoclaw software for depth-averaged flows with adaptive refinement. *Adv Water Resour* 24:1195–1206
- Blaise S, St-Cyr A, Mavriplis D, Lockwood B (2013) Discontinuous Galerkin unsteady discrete adjoint method for real-time efficient tsunami simulations. *J Comput Phys* 232
- Borrero JC, LeVeque RJ, Greer D, O'Neill S, Davis BN (2015) Observations and modelling of tsunami currents at the Port of Tauranga, New Zealand. In: Australasian Coasts & Ports Conference 2015, Engineers Australia and IPENZ, pp 90–95
- Buffoni G, Cupini E (2001) The adjoint advection-diffusion equation in stationary and time dependent problems: a reciprocity relation. *Rivista di Matematica della Universita di Parma* 4:9–19
- Bunge HP, Hagelberg CR, Travis BJ (2003) Mantle circulation models with variational data assimilation: inferring past mantle flow and structure from plate motion histories and seismic tomography. *Geophys J Int* 152:280–301
- Clawpack Development Team (2015) Clawpack software. URL <http://www.clawpack.org>, version 5.3
- Davis BN (2015) Adjoint code repository. URL <https://github.com/BrisaDavis/adjoint>
- Flynt BT, Mavriplis DJ (2012) Discrete adjoint based adaptive error control in unsteady flow problems. AIAA Paper 2012-0078
- GeoClaw Development Team (Accessed 2016) GEOCLAW software. <http://www.clawpack.org/geoclaw>
- George DL (2008) Augmented Riemann solvers for the shallow water equations over variable topography with steady states and inundation. *J Comput Phys* 227:3089–3113

- Giles MB, Pierce NA (2000) An introduction to the adjoint approach to design. *Flow Turbul Combust* 65(3-4):393–415
- Giles MB, Suli E (2002) Adjoint methods for pdes: a posteriori error analysis and postprocessing by duality. *Acta Numerica* 11:145–236
- González FI, LeVeque RJ, Adams LM, Goldfinger C, Priest GR, Wang K (2014) Probabilistic Tsunami Hazard Assessment (PTHA) for Crescent City, CA. URL <https://digital.lib.washington.edu/researchworks/handle/1773/25916>
- Grothe P, Taylor L, Eakins B, Carignan K, Caldwell R, Lim E, Friday D (2011) Digital Elevation Models of Crescent City, California: Procedures, Data Sources and Analysis. NOAA Technical Memorandum NESDIS NGDC-51, U.S. Dept. of Commerce, Boulder, CO, URL <http://www.ngdc.noaa.gov/dem/squareCellGrid/download/693>
- Hall MCG (1986) Application of adjoint sensitivity theory to an atmospheric general circulation model. *J Atmos Sci* 43:2644–2652
- Jameson A (1988) Aerodynamic design via control theory. *J Sci Comput* 3(3):233–260
- Kast SM, Fidkowski KJ (2013) Output-based mesh adaptation for high order navier-stokes simulations on deformable domains. *J Comput Phys* pp 468–494
- Kennedy GJ, Martins JRRA (2013) An adjoint-based derivative evaluation method for time-dependent aeroelastic optimization of flexible aircraft. In: *Proceedings of the 54th AIAA/ASME/ASCE/AHS/ASC Structures, Structural Dynamics, and Materials Conference*, Boston, MA, aIAA-2013-1530
- LeVeque RJ (2002) *Finite Volume Methods for Hyperbolic Problems*. Cambridge University Press
- LeVeque RJ, George DL, Berger MJ (2011) Tsunami modeling with adaptively refined finite volume methods. *Acta Numerica* pp 211–289
- Luo Y, Fidkowski KJ (2011) Output-based space-time mesh adaptation for unsteady aerodynamics. *AIAA Paper* 2011-491
- Mani K, Mavriplis DJ (2007) Discrete adjoint based time-step adaptation and error reduction in unsteady flow problems. *AIAA Paper* 2007-3944
- Marburger J (2012) Adjoint-based optimal control of time-dependent free boundary problems. URL <http://arxiv.org/abs/1212.3789>
- Mishra A, Mani K, Mavriplis D, Sitaraman J (2013) Time-dependent adjoint-based optimization for coupled aeroelastic problems. In: *31st AIAA Applied Aerodynamic Conference*, San Diego, CA, aIAA 2013-2906
- Othmer C (2014) Adjoint methods for car aerodynamics. *Journal of Mathematics in Industry* 4(1):6
- Park MA (2004) Adjoint-based, three-dimensional error prediction and grid adaptation. *AIAA Journal* 42:1854–1862
- Pierce NA, Giles MB (2000) Adjoint recovery of superconvergent functionals from pde approximations. *SIAM Review* 42:247–264
- Sanders BF, Katopodes ND (2000) Adjoint sensitivity analysis for shallow-water wave control. *J Eng Mech* 126(9):909919
- Tang L, Chamberlin C, Tolkova E, Spillane M, Titov VV, Bernard EN, Mofjeld HO (2006) Assessment of potential tsunami impact for Pearl Harbor, Hawaii. NOAA Technical Memorandum OAR PMEL-131
- Tromp J, Tape C, Liu Q (2005) Seismic tomography, adjoint methods, time reversal and banana-doughnut kernels. *Geophys J Int* 160:195–216

-
- Venditti DA, Darmofal DL (2000) Adjoint error estimation and grid adaptation for functional outputs: Application to quasi-one-dimensional flow. *J Comput Phys* 164:204–227
- Venditti DA, Darmofal DL (2002) Grid adaptation for functional outputs: application to two-dimensional inviscid flows. *J Comput Phys*
- Venditti DA, Darmofal DL (2003) Anisotropic grid adaptation for functional outputs: application to two-dimensional viscous flows. *J Comput Phys*
- Wang Q, Moin P, Iaccarino G (2009) Minimal repetition dynamic checkpointing algorithm for unsteady adjoint calculation. *SIAM J Sci Comput* 31(4):2549–2567